

# A correlation between unabsorbed hard X-rays and neutrinos in radio-loud and radio-quiet AGN

Emma Kun

*Astronomical Institute, Faculty for Physics & Astronomy,  
Ruhr University Bochum, 44780 Bochum, Germany  
Theoretical Physics IV: Plasma-Astroparticle Physics,  
Faculty for Physics & Astronomy, Ruhr University Bochum, 44780 Bochum, Germany  
Ruhr Astroparticle And Plasma Physics Center (RAPP Center),  
Ruhr-Universität Bochum, 44780 Bochum, Germany  
Konkoly Observatory, HUN-REN Research Centre for Astronomy and Earth Sciences,  
Konkoly Thege Miklós út 15-17, H-1121 Budapest, Hungary and  
CSFK, MTA Centre of Excellence, Konkoly Thege Miklós út 15-17, H-1121 Budapest, Hungary\**

Imre Bartos

*Department of Physics, University of Florida, PO Box 118440, Gainesville, FL 32611-8440, USA<sup>†</sup>*

Julia Becker Tjus

*Theoretical Physics IV: Plasma-Astroparticle Physics,  
Faculty for Physics & Astronomy, Ruhr University Bochum, 44780 Bochum, Germany  
Ruhr Astroparticle And Plasma Physics Center (RAPP Center),  
Ruhr-Universität Bochum, 44780 Bochum, Germany and  
Department of Space, Earth and Environment, Chalmers University of Technology, SE-412 96 Gothenburg, Sweden*

Peter L. Biermann

*MPI for Radioastronomy, 53121 Bonn, Germany and  
Department of Physics & Astronomy, University of Alabama, Tuscaloosa, AL 35487, USA*

Anna Franckowiak

*Astronomical Institute, Faculty for Physics & Astronomy,  
Ruhr University Bochum, 44780 Bochum, Germany*

Francis Halzen

*Department of Physics, University of Wisconsin, Madison, WI 53706, USA*

Santiago del Palacio

*Department of Space, Earth and Environment, Chalmers University of Technology, SE-412 96 Gothenburg, Sweden*

Jooyun Woo

*Columbia Astrophysics Laboratory, 550 West 120th Street, New York, NY 10027, USA*

(Dated: August 1, 2024)

The first high-energy neutrino source identified by IceCube was a blazar – an active galactic nucleus driving a relativistic jet towards Earth. Jets driven by accreting black holes are commonly assumed to be needed for high-energy neutrino production. Recently, IceCube discovered neutrinos from Seyfert galaxies, which appears unrelated to jet activity. Here, we show that the observed luminosity ratios of neutrinos and hard X-rays from blazars TXS 0506+056 and GB6 J1542+6129 are consistent with neutrino production in a  $\gamma$ -obscured region near a central supermassive black hole, with the X-ray flux corresponding to reprocessed  $\gamma$ -ray emission with flux comparable to that of neutrinos. Similar neutrino–hard X-ray flux ratios are found for four Seyfert galaxies, NGC 1068, NGC 4151, CGCG 420-015 and NGC 3079, raising the possibility of a common neutrino production mechanism that may not involve a strong jet.

The IceCube Neutrino Observatory has already made a series of transformational discoveries. These include a quasi-diffuse flux of cosmic neutrinos of so-far unknown

origin [1], as well as a growing number of individual astrophysical sites with associated neutrino emission.

The first individual neutrino source identified at  $> 3\sigma$  significance was the blazar TXS 0506+056 [2]. Blazars represent a special class of active galactic nuclei (AGN) that drive relativistic jets that point directly towards Earth. Relativistic jets can be sources of high-energy

---

\* ekun@astro.ruhr-uni-bochum.de

† imrebartos@ufl.edu

neutrinos if their accelerated protons undergo  $p\gamma$  or  $pp$  interactions [see e.g., 3–6], however, for the latter external material [7] or structured jets are needed [8]. The second neutrino source identified with high confidence was the Seyfert galaxy NGC 1068 [9]. Seyfert galaxies are radio-quiet AGNs with much weaker jets compared to blazars. Their hard X-ray emission likely originates from the hot plasma called corona surrounding the accretion disk of the central black hole in AGN.

Subsequently, additional astrophysical sources have been associated with neutrino emission. These included two blazars (PKS 1502+106, [10]; PKS 1424–41, [11]) and three Seyfert galaxies [NGC 4151, NGC 3079 CGCG 420-015; 12–14]. Additional neutrino source candidates include the blazars PKS 1424+240 ( $3.7\sigma$ ) and GB6 J1542+6129 ( $2.2\sigma$ ) [9]. Similarly to TXS 0506+056, these two blazars also possibly belong to a class of masquerading BL Lac objects [15].

High-energy neutrinos are produced through the interactions of relativistic protons accelerated in the sources. These interactions also produce  $\gamma$ -rays with comparable flux and energy spectra to that of neutrinos. However, if such interactions take place near the central black hole, where plenty of infrared-optical photons from the accretion disk and X-rays from the hot corona are present, active pair-production will convert, or reprocess, the  $\gamma$ -rays into  $\lesssim 1$  MeV photons (hard X-rays) [13, 16–18]. The apparent underproduction of  $\gamma$ -rays compared to neutrinos in Seyfert galaxies is naturally explained in such environments [e.g., 19, 20]. Even blazars, generally bright  $\gamma$ -ray sources, tend to show a temporary  $\gamma$ -opaqueness during neutrino emission. A hint of  $\gamma$ -absorption is also observed in the diffuse neutrino flux [16, 21].

Consequently, hard X-ray emission produced by this reprocessing should have comparable flux to that of high-energy neutrinos. The linear scaling between the *unabsorbed* hard X-ray and neutrino fluxes for Seyfert galaxies has already been suggested by [22]. Based on this linear scaling and observations in the 2–10 keV band, Murase *et al.* [16] listed the brightest neutrino source candidate AGNs including NGC 1068. The AGNs NGC 1068 [ $z = 0.003810$ , 23], NGC 3079 [ $z = 0.00399$ , 24] and NGC 4151 [ $z = 0.003152$ , 24] were indeed suggested to have comparable *unabsorbed* hard X-ray (15–195 keV range) and all-flavor neutrino fluxes [13].

## I. HARD X-RAY FLUXES

Due to significant reprocessing by multiple Compton scatterings and photoelectric absorption in Seyfert galaxies, complicated obscurer models (e.g., MYTorus [25, 26]) are often adopted to account for such reprocessing of X-rays and calculate the *unabsorbed* flux. Neronov *et al.* [13], however, used a simple exponential absorption correction and a power-law model to convert the *observed* hard X-ray flux.

We estimated the *unabsorbed* hard X-ray flux of the

four IceCube-detected Seyfert galaxies, namely NGC 1068, NGC 4151, NGC 3079 and CGCG 420-015 to deduce a physically appropriate relation between their hard X-ray and neutrino flux. We extended this comparison to the all-time average of the blazar TXS 0506+056 [ $z = 0.3365$ , 27], the only blazar with neutrino flux identified with  $> 3\sigma$  confidence.

We additionally carried out an X-ray observation of the blazar GB6 J1542+6129 using the NuSTAR X-ray satellite. GB6 J1542+6129 is another blazar associated with IceCube neutrinos. We corroborate that the X-ray absorption in the Galactic interstellar medium is significantly smaller than the intrinsic absorption for these AGN, the Galactic hydrogen column density being in the order of  $\sim 10^{20}$  cm $^{-2}$  [28–30].

Regarding the hard X-ray flux of NGC 1068, we extrapolated the 10–40 keV Nuclear Spectroscopic Telescope Array [*NuSTAR*, 31] unabsorbed luminosity  $L_{10-40, \text{intr}} \approx 1.5 \times 10^{43}$  erg s $^{-1}$  from Bauer *et al.* [32] to the 15–55 keV range, with the spectral index  $\Gamma = 2.10 \pm 0.07$ . The resulted luminosity of the main continuum is  $L_{15-55, \text{intr}} \approx 1.36 \pm 0.15 \times 10^{43}$  erg s $^{-1}$ , where we assumed a 10% error on the 10–40 keV luminosity.

For NGC 3079, assuming an edge-on configuration, Marchesi *et al.* [33] favors a value of  $2.47 \pm 0.24 \times 10^{24}$  cm $^{-2}$  for  $N_H$  (along the line-of-sight), which is in agreement with the value  $N_H = 3.2_{-0.43}^{+0.54} \times 10^{24}$  cm $^{-2}$  suggested by Georgantopoulos and Akylas [34], also relying on *NuSTAR* observations. We adopt the luminosity of the main continuum of NGC3079 of  $L_{15-55, \text{intr}} = 2.63_{-0.59}^{+0.61} \times 10^{42}$  erg s $^{-1}$ , from Marchesi *et al.* [33].

In the case of NGC 4151, the favored in-source column density is  $N_H \sim 10^{22-10^{23}}$  cm $^{-2}$  [e.g. 35, 36], or even smaller. Gianolli *et al.* [37] gives the parameters for the Comptonized primary continuum of NGC 4151; we retrieved the 15–55 keV flux by loading in XSPEC the `nthcomp` model with their fitted parameters, obtaining an unabsorbed flux of  $F_{15-55} \approx 3.1 \times 10^{-10}$  erg s $^{-1}$  cm $^{-2}$ .

The unabsorbed hard X-ray luminosity of CGCG 420-015 [ $z=0.0296$ , 38] was estimated by Marchesi *et al.* [33] as  $\log(L_{15-55, \text{intr}}) = 43.65_{-0.12}^{+0.09}$  erg s $^{-1}$  with a line-of-sight column density of  $N_H = 7.15_{-0.97}^{+0.85} \times 10^{23}$  cm $^{-2}$ .

As a broadband (3–79 keV) focused (FWHM 14”) hard X-ray space telescope, *NuSTAR* has been providing unique opportunities to study extreme phenomena of AGNs in the X-ray band including TXS 0506+056. We analyzed all available *NuSTAR* data of TXS 0506+056, consisting of 18 observations between 2017 and 2021 with a total exposure of 371 ks. We processed the data using NuSTAR Data Analysis Software (NuSTARDAS v2.1.2) and CALDB 20230718. We generated cleaned data products using `nupipeline` task with `saamode=strict` and `tentacle=yes` flags. Source (background) spectra were extracted from a circular region with radius 30” (annular region with radius 1’.5–2’.5) centered at TXS 0506+056. The source is bright over the background in 3 to  $\sim 40$  keV for all observations. We modeled the spectra from each observation separately with an absorbed redshifted power

law (`tbabs*zpow`) in XSPEC [39] using the Galactic hydrogen column density ( $N_{\text{H}} = 1.55 \times 10^{21} \text{ cm}^{-2}$ ), the abundance table from Wilms *et al.* [40] (`abund wilm`), and redshift  $z = 0.3365$  [27]. The power law index varies between 1.5 – 1.9 among observations. The source is variable in the hard X-ray roughly within a factor of  $\sim 2$  as reported in Acciari *et al.* [41]. The list of observations and 15–55 keV luminosity for each observation is shown in Table I in Appendix A. To provide observational window for the X-ray luminosity comparable to the integrated neutrino luminosity, we calculated the luminosity of TXS 0506+056 by averaging the luminosity measurement from all the available observations. The average 15–55 keV luminosity of TXS 0506+056 is  $(9.0 \pm 2.4) \times 10^{44} \text{ erg s}^{-1}$ , where we adopted the  $1\sigma$  quartile of the flux distribution as the errorbar to account for variability.

The blazar GB6 J1542+6129 ( $z = 0.507$ , [42]) was observed first time by *NuSTAR* Program 10049 (PI del Palacio) with a 36 ks exposure. We generated cleaned data products using `nupipeline` task with `saacalc=2`, `saamode=optimized` and `tentacle=yes` flags. The source spectrum was extracted from a circular region with radius 30" centered on GB6 J1542+6129 and the background was chosen from a larger ellipsoidal region in a source-free region within the same chip. GB6 J1542+6129 is detected significantly above the background up to  $\sim 20$  keV. As done with TXS 0506+056, we modeled the spectrum with an absorbed redshifted power law (`tbabs*zpow`) in XSPEC, although the absorption is negligible due to the low column density towards this source ( $N_{\text{H}} = 0.13 \times 10^{21} \text{ cm}^{-2}$ ). The powerlaw photon index is  $\Gamma = 1.55 \pm 0.15$ , which is significantly harder than the spectral index inferred from *Swift*-XRT observations ( $\Gamma \sim 2.5$ ). The model yields a flux in the 15–55 keV energy range of  $F_{15-55} = (6.0 \pm 1.2) \times 10^{-13} \text{ erg s}^{-1} \text{ cm}^{-2}$ . We note that the lightcurve obtained with *Swift*-XRT [43] for this sources does not exhibit strong flaring variability, suggesting that the X-ray emission from GB6 J1542+6129 is relatively steady within a factor  $\sim 2$ , and therefore the reported flux should be representative of the source flux in the 10-yr IceCube window.

## II. HIGH-ENERGY NEUTRINO FLUXES

For three Seyfert galaxies NGC 1068, NGC 4151, NGC 3079, we assumed the high-energy neutrino fluxes reported by Neronov *et al.* [13]. All neutrino spectrums are assumed to be a power-law in the form of  $\phi_{\nu}(E) = \phi_0 (E_{\nu}/E_0)^{-\gamma}$ , where  $\phi_0$  is the normalization factor and  $\gamma$  is the spectral index ( $E_0 = 1 \text{ TeV}$ ). We note all analyses use similar amount of neutrino data.

In the case of CGCG 420-015, we estimated the 0.3–100 TeV integrated neutrino flux from the best-fit normalization factor ( $\phi_0 \approx 1.2 \times 10^{-11} \text{ TeV}^{-1} \text{ cm}^{-2} \text{ s}^{-1}$ ) and spectral index ( $\hat{\gamma} \approx 2.8$ ) based on the likelihood scan

from Abbasi *et al.* [14]. Then the integrated flux emerges as  $F_{\nu_{\mu}+\bar{\nu}_{\mu}} = (3.8 \pm 2.5) \times 10^{-12} \text{ TeV cm}^{-2} \text{ s}^{-1}$ , which comes from

$$F_{\nu_{\mu}+\bar{\nu}_{\mu}} = \int_{E_1}^{E_2} E_{\nu} \phi_{\nu_{\mu}+\bar{\nu}_{\mu}}(E_{\nu}) dE, \quad (1)$$

with  $E_1 = 0.3 \text{ TeV}$  and  $E_2 = 100 \text{ TeV}$ .

We estimated the 0.3–100 TeV integrated neutrino flux of TXS 0506+056 from Abbasi *et al.* [9]. We derived  $\phi_{\nu_{\mu}+\bar{\nu}_{\mu}}$  such that  $\phi_0 \approx 3.57 \times 10^{-13} \text{ TeV}^{-1} \text{ cm}^{-2} \text{ s}^{-1}$  and  $\hat{\gamma} \approx 2.04$ . We estimated the relative error of the resulted flux considering the 68% confidence interval at the 100 TeV energy. Then the integrated neutrino flux between 0.3 TeV and 100 TeV results as  $F_{\nu_{\mu}+\bar{\nu}_{\mu}} = 1.93 \times 10^{-12} \text{ TeV cm}^{-2} \text{ s}^{-1}$ , with lower and upper limits of  $1.70 \times 10^{-13} \text{ TeV cm}^{-2} \text{ s}^{-1}$  and  $4.70 \times 10^{-12} \text{ TeV cm}^{-2} \text{ s}^{-1}$ , respectively.

In the case of GB6 J1542+6129, the best-fit number of signal events ( $\hat{n}_s = 16.0$ ) and astrophysical spectral index ( $\hat{\gamma} = 3.0$ ) are published [9]. The number of signal events  $n_s$  detected by IceCube from a source in direction of declination  $\delta$  is given as:

$$n_s = \tau \int_0^{\infty} A_{\text{eff}}(E_{\nu}, \delta) \times \phi_{\nu_{\mu}+\bar{\nu}_{\mu}}(E_{\nu}) dE \quad (2)$$

where  $\tau$  is the livetime,  $A_{\text{eff}}(E_{\nu}, \delta)$  is the energy and direction dependent effective area of the detector ( $\delta_{\text{GB6 J1542+6129}} = 61.5^\circ$ ). The published tabulated effective areas of the IceCube Neutrino Detector range from  $E_{\text{min}} = 100 \text{ GeV}$  to  $E_{\text{max}} = 10 \text{ PeV}$ , in 40 log-scale bins [seasons: IC40, IC59, IC79, IC86-I, IC86-II in 44]. Then the number of signal events summing over in all seasons is

$$n_s = \phi_0 \sum_{n=1}^5 \tau_n \left( \sum_{i=1}^{40} A_{\text{eff},i} \int_{E_{l,i}}^{E_{u,i}} \left( \frac{E_{\nu}}{E_0} \right)^{-\gamma} dE \right)_n \quad (3)$$

where  $i$  the energy bin number running from 1 to 40,  $\tau_1$ – $\tau_5$  are the seasons's livetimes,  $E_{l,i}(E_{u,i})$  is the lower(upper) energy of the  $i$ th energy bin and  $n$  the season number running from 1 to 5. Reorganizing the equation we get  $\phi_0 = 1.5 \times 10^{-12} \text{ TeV}^{-1} \text{ cm}^{-2} \text{ s}^{-1}$  (this is about the 90% upper limit given by IceCube) and the 0.3–100 TeV integrated neutrino flux of GB6 J1542+6129 arises as  $F_{\nu_{\mu}+\bar{\nu}_{\mu}} = 5.0 \pm 3.8 \times 10^{-12} \text{ TeV cm}^{-2} \text{ s}^{-1}$ . This flux is about 2.5 times larger compared to TXS 0506+056 in the 0.3–100 TeV range, which can be explained with the larger  $\hat{n}_s$  and softer  $\hat{\gamma}$  of GB6 J1542+6129. We note that to be compatible with Neronov *et al.* [13], who gave the  $F_{\nu_{\mu}}$ , we did take account only for the muon component by halving the above fluxes.

## III. $\gamma$ -OBSCURED NEUTRINO SOURCES

We show our results in the left side of Fig. 1, where one can see a possible correlation between the unabsorbed hard X-ray and neutrino luminosities of the four

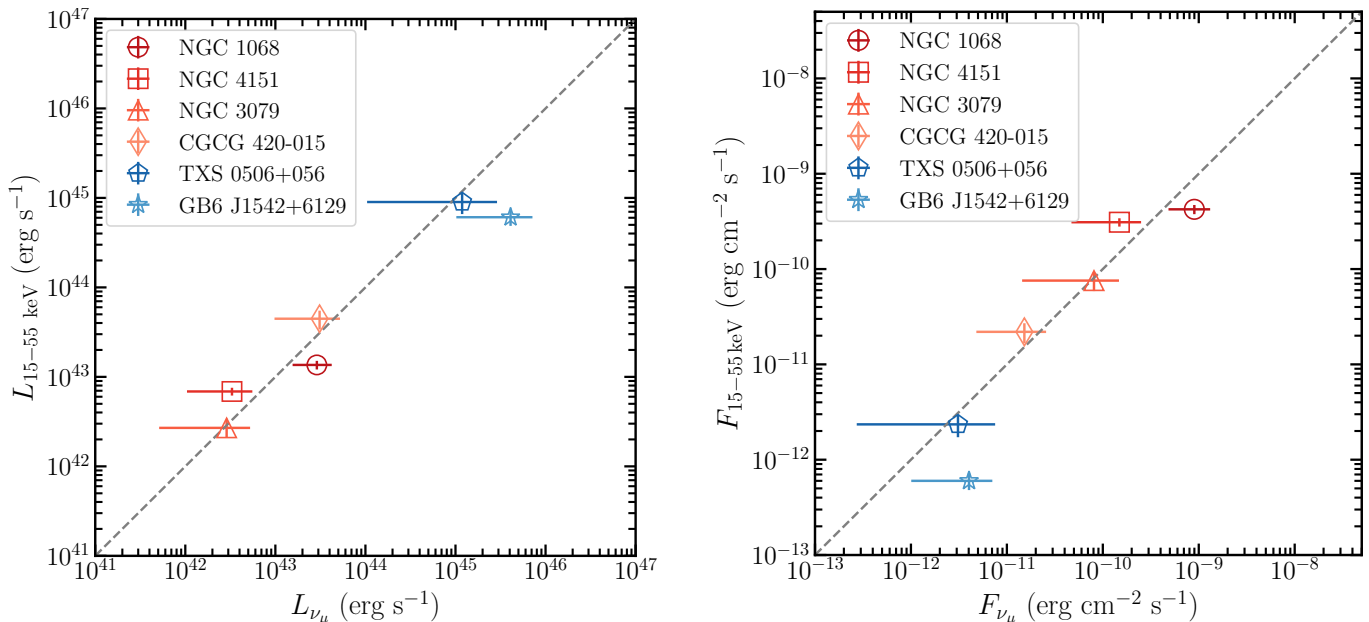


FIG. 1. Correlation plot between the unabsorbed hard X-rays and neutrinos in radio-loud and radio-quiet AGN in our sample. Left: Luminosity of the main (unabsorbed) hard X-ray continuum shown as a function of the high-energy neutrino flux for four Seyferts, NGC 1068, NGC 4151, NGC 3079, CGCG 420-015 in red, and the blazars TXS 0506+056 and GC6 J1542+6129 in blue. The dashed line shows  $L_X = L_\nu$ . Right: the same as on the left plot, but in fluxes.

Seyfert galaxies and the two blazar in our AGN sample. The same relation can be seen for between the hard X-ray and neutrino fluxes (right side of Fig. 1,  $H_0 = 69.6 \text{ km s}^{-1} \text{ Mpc}^{-1}$ ,  $\Omega_{\text{m},0} = 0.286$ ,  $\Omega_{\lambda,0} = 0.714$ ,  $T_{\text{cmb},0} = 2.72548 \text{ K}$  in a  $\Lambda$ CDM cosmology), which might be due to the still relatively small sample size. The Pearson correlation-index between the logarithm of luminosities emerges as  $R = 0.966$  hinting at strong linear correlation, though the small number of elements in the sample prevents deeper investigations. We would like to emphasize that this plot shows for the first time the possibility that signatures from blazars might have the same origin as the Seyferts, which is a very different scientific point compared to Neronov *et al.* [13].

An important point is to understand the level of contribution of the jet component to the hard X-ray emission, especially in the case of TXS 0506+056. We show in the Appendix B that using only those *NuSTAR* observations on TXS 0506+056 that were taken during the low very high-energy activity phase of TXS 0506+056 as measured by MAGIC [ $E > 90 \text{ GeV}$ , 45], the resulted hard X-ray luminosity ( $(6.6 \pm 0.9) \times 10^{44} \text{ erg s}^{-1}$ ) does not differ significantly from the mean one in Fig. 1 ( $(9.0 \pm 2.4) \times 10^{44} \text{ erg s}^{-1}$ , taking into account all *NuSTAR* observations). Adding to the picture that the *Fermi-LAT*  $\gamma$ -ray emission goes down while the *NuSTAR* hard X-ray emission goes up in the overlapping time period (see Fig. 2 in Appendix B), it is highly unlikely that the jet significantly contributes to the 15–55 keV hard X-rays of TXS 0506+056 (at least after 2017).

Comparable unabsorbed hard X-ray and neu-

trino luminosities for blazars TXS 0506+056 and GB6 J1542+6129, as well as four Seyfert galaxies suggests that neutrinos are produced in  $\gamma$ -obscured regions, such as their cores rather than along the jet, for all six sources (see Appendix C). It has been shown by Murase [46] that the linear scaling between  $L_X$  and  $L_\nu$  in Seyfert/low-luminosity (LL) AGN systems holds while  $t^* \approx R/V$  is longer than  $R/c$ , where  $R$  is the emission radius,  $V$  is the characteristic velocity in the plasma, and  $c$  is the speed of light in the medium (see their Eq. 5 defining the photomeson production optical depth). For non-relativistic sources such as AGN coronae, the optical depth for the photomeson production can be larger by a factor of 10–100.

#### IV. COMMON ORIGIN?

AGNs can produce neutrinos without Earth-pointing relativistic jets. It is tempting to investigate whether a mechanism that does not require a jet pointing towards Earth, could be behind neutrino emission in blazars such as TXS 0506+056.

One possible clue can be the  $\sim 1 \text{ MeV}$  photon cut-off energy and the corresponding electromagnetic energy release in hard X-rays, which is natural in  $\gamma$ -ray attenuated AGN core environments but it is not justified in jets. For example, the observed hard X-ray flux during the neutrino-bright phase of TXS 0506+056 is well described by a lepto-hadronic model predicting a monotonically increasing flux to the GeV  $\gamma$ -ray band [47]. While

current observations are not sensitive to probe the possible  $\sim 1$  MeV cutoff for TXS 0506+056, the comparable unabsorbed hard X-ray luminosity to that of the neutrinos supports a significant  $\gamma$ -ray energy release to the sub-MeV band.

Second, blazars can produce detectable very high-energy (VHE,  $> 100$  GeV)  $\gamma$ -rays [e.g. the VHE-phases of TXS 0506+056 presented in 45]. The escape of these VHE photons conflicts the apparent  $\gamma$ -obscured neutrino production that is needed by the comparable hard X-ray and neutrino fluxes. A possible reconciliation of VHE emission by blazar jets can be the temporal variability of  $\gamma$  attenuation. When the jet is in a VHE-active phase, the Doppler-boosted jet outshines the corona/accretion disk, however, the same cannot happen for neutrinos. The temporal  $\gamma$  suppression in jets is also consistent with the observed dip in  $\gamma$  emission around neutrino observations reported for several blazars [20, 48].

One additional clue may be the relative luminosities of the observed neutrino sources. TXS 0506+056 appears to be  $\sim 2$  orders of magnitude brighter than the four Seyfert galaxies considered here (both in neutrinos and hard X-rays; see Fig. 1), which might be internal or external to the core (e.g. jet viewing angle). Supermassive black holes (SMBHs) in blazars appear to have 1-2 orders of magnitude larger mass compared to the SMBHs in local galaxies. Since the luminosity scales with the total mass of the SMBH, this difference in the total masses naturally would resolve the difference in luminosities, however, at this point this is only a speculation and further investigation is needed.

Another difference of note is the neutrino spectrum. The 2014–2015 burst of TXS 0506+056 appears to produce neutrino spectrum of  $dN/dE \propto E_\nu^{-2.2}$  [49]. This is in contrast of the steeper spectra of, e.g., NGC 1068 which has a spectrum of  $dN/dE \propto E_\nu^{-3.3}$  [9]. The reason is possibly that in the case of TXS 0506+056 we are observing high-energy neutrinos produced by  $p\gamma$  interactions (e.g., Stecker and Salamon [50]), while somewhat lower energy neutrinos in NGC 1068 are produced via  $pp$  interactions (e.g., Murase *et al.* [16]).

Finally, the emission's temporal variation of multi-messenger events may help differentiate between a jet and non-jet origin. For example, neutrinos were detected from TXS 0506+056 in effectively two distinct emission episodes, in 2014/2015 and 2017 [49]. While the 2017 detection coincided with a several months-long  $\gamma$  flare, TXS 0506+056 had low  $E_\gamma > 100$  MeV flux during the 2015 emission episode [49]. Radio flux was roughly constant throughout of the 2014/2015 episode, suggesting that changes in the relativistic outflow by itself do not account for the varying neutrino flux, rather the energy excess was suppressed already in the corona and did not reach the radio jet base.

Gopal-Krishna and Biermann [51] pointed out that winds and jets all carry an electric current. If the jets or winds vary with time, and they all do, then the temporal variation of the electric currents produces tempo-

rary electric fields. These fields discharge, producing energetic particles with spectra between  $p^{-2}$  and  $p^{-4}$  for hadrons and  $p^{-3}$  and  $p^{-5}$  for electrons/positrons, in the Kardashev [52] loss limit. This gives a spectral range in synchrotron emission in the range between  $\nu^{-1}$  and  $\nu^{-2}$ , which is widely observed in radio filaments, both Galactic and extragalactic.

## V. CONCLUSION

We found that the unabsorbed hard X-ray and high-energy neutrino luminosities of blazar TXS 0506+056 are comparable. This is similar to the relation for Seyfert galaxies NGC 1068, NGC 4151, CGCG 420-015 and NGC 3079 (see left panel in Fig. 1). Another blazar, GB6 J1542+6129 also seems to be close to the relation. This relation for Seyfert galaxies was initially found by [13], but here we recalculate it using hard X-ray flux measurements from *NuSTAR* observations in the literature.

Our results suggest the following:

1. The comparable unabsorbed hard X-ray and neutrino luminosities in our sample is consistent with neutrino production in  $\gamma$ -obscure regions with photons attenuated down to  $\sim 1$  MeV energies.
2. The same astrophysical process might be responsible for neutrino production in blazars and Seyfert AGNs. Photon attenuation to  $\sim 1$  MeV is expected for neutrino production near AGN disks. In this case, neutrino production may not be dominated by jets, even in the case of blazars.
3. Hard X-rays are very promising targets for multi-messenger modeling of AGN in respect of neutrino-source searches.

We note that all of the potential classes of neutrino sources have the same astrophysical nature: accreting supermassive black holes. Since neutrino emission from Seyfert galaxies is unlikely to be related to their weak jets, a natural question arises as to whether neutrino emission from blazars could also have an origin besides their powerful jets, such as near the central black hole.

We caution nonetheless that the comparable X-ray and neutrino fluxes we found are both subject to uncertainties due to, e.g., emission's spectral uncertainty and possible temporal variations. Challenges include the generally weak and not well time-constrained neutrino signal versus X-ray observation window, the more sophisticated determination of the unabsorbed hard X-ray flux, sample size. It will be particularly interesting to determine whether a similar relation holds for other identified sources of high-energy neutrinos, and whether multi-messenger emission and spectral features can be used to distinguish between the disk/corona and jet origins of neutrinos. We encourage deep hard X-ray / soft- $\gamma$ -ray observations of these sources.

TABLE I. *NuSTAR* observations used to calculate the hard X-ray vs. high-energy neutrino flux relation.

ObsID	Date	Exposure (ks)	$L_{15-55}$ ( $10^{44}$ erg s $^{-1}$ )
90301618002	2017-09-29	21.6	$6.5 \pm 0.8$
90301618004	2017-10-19	19.7	$6.6 \pm 0.9$
90401610002	2018-04-03	2.2	$10.6 \pm 1.1$
90402637002	2018-10-16	26.5	$10.7 \pm 0.9$
90402637004	2018-11-15	22.9	$7.0 \pm 0.9$
90402637006	2018-12-08	20.8	$8.3 \pm 0.9$
90402637008	2019-01-07	1.9	$10.9 \pm 1.0$
60502053002	2019-07-30	17.4	$13.3 \pm 1.2$
60502053004	2019-09-29	25.9	$10.1 \pm 0.9$
60502053006	2019-11-29	17.7	$10.8 \pm 1.2$
60502053008	2020-01-26	15.1	$9.5 \pm 1.2$
60502053010	2020-03-25	20.8	$12.3 \pm 1.1$
60602004002	2020-09-26	18.3	$9.7 \pm 1.1$
60602004004	2020-10-25	22.0	$12.3 \pm 1.2$
60602004006	2020-11-17	20.4	$7.9 \pm 0.9$
60602004008	2020-12-10	20.1	$6.7 \pm 0.9$
60602004010	2021-01-16	17.5	$4.0 \pm 0.8$
60602004012	2021-02-12	22.8	$5.1 \pm 0.7$
Total exposure		370.7	
Average luminosity in 15–55 keV			$9.0 \pm 0.2$

## ACKNOWLEDGMENTS

The authors thank the Referees for the thoughtful and constructive points. The authors also would like to thank Björn Eichmann, Stefano Marchesi, Sera Markoff, Kohta Murase, Claudio Ricci, Walter Winter and Xiurui Zhao for valuable discussions. E.K. thanks the Alexander von Humboldt Foundation for its Fellowship. J.B.T. E.K., and A.F. acknowledge support from the German Science Foundation DFG, via the Collaborative Research Center *SFB1491: Cosmic Interacting Matters – from Source to Signal* (grant no. 445052434). S.d.P. acknowledges support from ERC Advanced Grant 789410. This research has made use of the *NuSTAR* Data Analysis Software (*NuSTARDAS*) jointly developed by the ASI Space Science Data Center (SSDC, Italy) and the California Institute of Technology (Caltech, USA). This work made use of data supplied by the UK Swift Science Data Centre at the University of Leicester. This work made use of Astropy: <http://www.astropy.org>, a community-developed core Python package and an ecosystem of tools and resources for astronomy [53, 54].

### Appendix A: List of *NuSTAR* observations on TXS 0506+056 employed in this work

Here we give the list of *NuSTAR* observations that we used to derive the unabsorbed hard X-ray luminosity of TXS 0506+056.

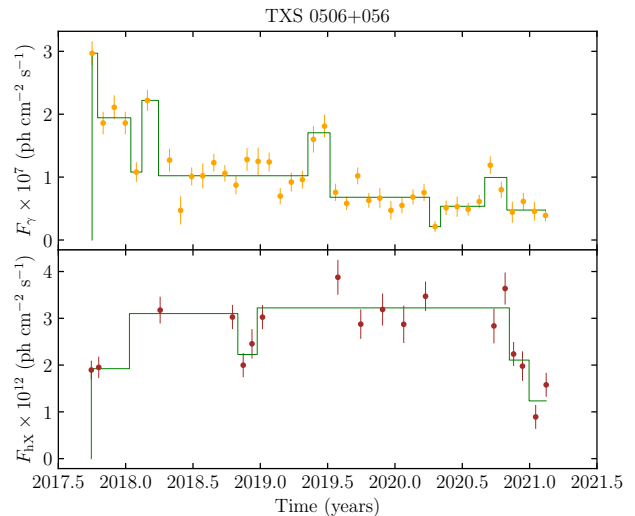


FIG. 2. The upper panels shows the 0.1–100 GeV *Fermi*-LAT one-month binned  $\gamma$ -ray light curve of TXS 0506+056 from the *Fermi* Light Curve Repository [57] (orange dots with errorbars) and the Bayesian blocks with  $p = 0.05$  (green line). The lower panels shows the 15–55 keV *NuSTAR* hard X-ray light curve of TXS 0506+056 (red dots with errorbars) and the Bayesian blocks with  $p = 0.05$  (green line). The purple dashed vertical line shows the detection time of the signal event IC-170922A.

### Appendix B: Does the jet significantly contribute to the hard X-ray flux of TXS 0506+056?

Ansoldi *et al.* [45] shows the high-energy MAGIC observations ( $E > 90$  GeV) on TXS 0506+056 in about 40 days from the detection time of the IceCube neutrino event IC-170922A. They identified two very-high energy (VHE) phases of TXS 0506+056, one between MJD 58029–58030 and a second one on MJD 58057. Sahakyan [56] modeled the broadband SED of TXS 0506+056 in these VHE phases and outside of them during low-VHE activity. In the VHE phase, when the jet is supposed to be active based on MAGIC, the soft X-ray flux measured by Swift-XRT was high. One can see that the boosted synchrotron/SSC emission from the jet steeply cuts off below 10 keV during the low-VHE phase. After the spectral hardening, the synchrotron emission from secondary  $e^-e^+$  pairs starts to rise. The first two *NuSTAR* observations on TXS 0506+056 (2017-09-29 and 2017-10-19) overlapped with the MAGIC observations, and the MAGIC flux was low during the *NuSTAR* epochs. The mean *NuSTAR* luminosity in these two epochs is  $(6.6 \pm 0.9) \times 10^{44}$  erg s $^{-1}$ , which does not differ significantly from the mean luminosity plotted in Fig. 1 ( $(9.0 \pm 2.4) \times 10^{44}$  erg s $^{-1}$ , corrected for variability, taking into account all *NuSTAR* observations). Another argument against a jet component dominating the hard X-ray emission shows up when comparing the 0.1–100 GeV *Fermi*-LAT [57] and *NuSTAR* light curves (*NuSTAR* started to observe TXS 0506+056 only after the

IC-170922A neutrino event). It seems that in the overlapping time period, the  $\gamma$ -ray emission, usually attributed to the jet component, goes down, while the hard X-ray emission goes up and maintains a high state, only dropping after the end of 2020 (see Fig. 2). We note that the background of TXS 0506+056 is usually strong at lower energies.

### Appendix C: Comparable hard X-ray and neutrino luminosity from $\gamma$ -obscured sources

Consider the case of protons accelerated near the black hole or in the accretion disk, interacting with a target photon field of characteristic size  $R_{\text{target}}$  centered at the black hole. In this ‘‘corona’’ region, which has large densities in both X-rays and accreting matter, the opacity to accelerated protons is [55]

$$\tau_{p\gamma} \simeq \frac{\kappa_{p\gamma} R_{\text{target}}}{\lambda_{p\gamma}} \simeq \kappa_{p\gamma} R_{\text{target}} \sigma_{p\gamma} n_{\gamma}, \quad (\text{C1})$$

determined by how many times a proton interacts in a target of size  $R_{\text{target}}$  given its interaction length  $\lambda_{p\gamma}$ ;  $\kappa_{p\gamma}$  is inelasticity, or the fraction of the energy a proton loses

with each interaction. The interaction length is determined by the density of target photons  $n_{\gamma}$  and the interaction cross section  $\sigma_{p\gamma}$ . For the simple dimensional analysis in this section we use the following cross sections  $\sigma_{\gamma\gamma} = 6.7 \times 10^{-25} \text{ cm}^2$ ,  $\sigma_{p\gamma} = 5 \times 10^{-28} \text{ cm}^2$ , and  $\sigma_{pp} = 3 \times 10^{-26} \text{ cm}^2$ .

The opacity of the target to the photons (pionic  $\gamma$ -rays) produced along with the neutrinos is given by

$$\tau_{\gamma\gamma} \simeq R_{\text{target}} \sigma_{\gamma\gamma} n_{\gamma}, \quad (\text{C2})$$

and therefore, approximately, the two opacities are related by their cross sections

$$\tau_{\gamma\gamma} \simeq \frac{\sigma_{\gamma\gamma}}{\kappa_{p\gamma} \sigma_{p\gamma}} \tau_{p\gamma} \simeq 10^3 \tau_{p\gamma} \quad (\text{C3})$$

for  $R_{\text{target}} \sim R$ , where  $R$  is the size of the injection region. There is an additional factor associated with the different thresholds of the two interactions [58]. A target that produces neutrinos with  $\tau_{p\gamma} \gtrsim 0.1$  will not be transparent to the pionic  $\gamma$ -rays, which will lose energy in the target even before propagating in the extragalactic background light.

- 
- [1] M. G. Aartsen, R. Abbasi, Y. Abdou, M. Ackermann, J. Adams, *et al.*, Phys. Rev. Lett. **111**, 021103 (2013), arXiv:1304.5356 [astro-ph.HE].
  - [2] IceCube Collaboration, Fermi-LAT, MAGIC, AGILE, ASAS-SN, HAWC, H.E.S.S., INTEGRAL, Kanata, Kiso, Kapteyn, Liverpool Telescope, Subaru, Swift/NuSTAR, VERITAS, and VLA/17B-403, Science **361**, 147 (2018).
  - [3] K. Mannheim, T. Stanev, and P. L. Biermann, A&A **260**, L1 (1992).
  - [4] J. K. Becker, P. L. Biermann, and W. Rhode, Astroparticle Physics **23**, 355 (2005), arXiv:astro-ph/0502089 [astro-ph].
  - [5] J. K. Becker, Phys. Rep. **458**, 173 (2008), arXiv:0710.1557 [astro-ph].
  - [6] J. Becker Tjus, B. Eichmann, F. Halzen, A. Kheirandish, and S. M. Saba, Phys. Rev. D **89**, 123005 (2014), arXiv:1406.0506 [astro-ph.HE].
  - [7] A. T. Araudo, V. Bosch-Ramon, and G. E. Romero, A&A **522**, A97 (2010), arXiv:1007.2199 [astro-ph.HE].
  - [8] F. Tavecchio and G. Ghisellini, MNRAS **451**, 1502 (2015), arXiv:1411.2783 [astro-ph.HE].
  - [9] R. Abbasi, M. Ackermann, J. Adams, J. A. Aguilar, M. Ahlers, M. Ahrens, J. M. Alameddine, C. Alispach, *et al.*, Science **378**, 538 (2022), arXiv:2211.09972 [astro-ph.HE].
  - [10] I. Taboada and R. Stein, The Astronomer’s Telegram **12967**, 1 (2019).
  - [11] M. Kadler, F. Krauß, K. Mannheim, R. Ojha, C. Müller, R. Schulz, G. Anton, W. Baumgartner, *et al.*, Nature Physics **12**, 807 (2016), arXiv:1602.02012 [astro-ph.HE].
  - [12] S. Goswami, arXiv e-prints, arXiv:2307.15349 (2023), arXiv:2307.15349 [astro-ph.HE].
  - [13] A. Neronov, D. Savchenko, and D. V. Semikoz, Phys. Rev. Lett. **132**, 101002 (2024).
  - [14] R. Abbasi, M. Ackermann, J. Adams, J. A. Aguilar, M. Ahlers, M. Ahrens, J. M. Alameddine, C. Alispach, *et al.*, <https://arxiv.org/abs/arXiv:2406.07601> arXiv: arXiv:2406.07601 [astro-ph.HE].
  - [15] P. Padovani, B. Boccardi, R. Falomo, and P. Giommi, MNRAS **511**, 4697 (2022), arXiv:2202.04363 [astro-ph.HE].
  - [16] K. Murase, S. S. Kimura, and P. Mészáros, Phys. Rev. Lett. **125**, 011101 (2020), arXiv:1904.04226 [astro-ph.HE].
  - [17] Y. Inoue, D. Khangulyan, and A. Doi, ApJ **891**, L33 (2020), arXiv:1909.02239 [astro-ph.HE].
  - [18] B. Eichmann, F. Oikonomou, S. Salvatore, R.-J. Dettmar, and J. Becker Tjus, Astrophys. J. **939**, 43 (2022), arXiv:2207.00102 [astro-ph.HE].
  - [19] E. Kun, I. Bartos, J. Becker Tjus, P. L. Biermann, A. Franckowiak, F. Halzen, and G. Mező, A&A **679**, 46 (2023), arXiv:2305.06729 [astro-ph.HE].
  - [20] E. Kun, I. Bartos, J. Becker Tjus, P. L. Biermann, F. Halzen, and G. Mező, ApJ **911**, L18 (2021), arXiv:2009.09792 [astro-ph.HE].
  - [21] K. Murase, D. Guetta, and M. Ahlers, Phys. Rev. Lett. **116**, 071101 (2016).
  - [22] K. Murase and E. Waxman, Phys. Rev. D **94**, 103006 (2016), arXiv:1607.01601 [astro-ph.HE].
  - [23] M. J. Meyer, M. A. Zwaan, R. L. Webster, L. Staveley-Smith, E. Ryan-Weber, M. J. Drinkwater, D. G. Barnes, M. Howlett, *et al.*, MNRAS **350**, 1195 (2004), arXiv:astro-ph/0406384 [astro-ph].
  - [24] M. J. Koss, B. Trakhtenbrot, C. Ricci, K. Oh, F. E.

- Bauer, D. Stern, T. Caglar, J. S. den Brok, *et al.*, *ApJS* **261**, 6 (2022), arXiv:2207.12435 [astro-ph.GA].
- [25] K. Mori, C. J. Hailey, R. Krivonos, J. Hong, G. Ponti, F. Bauer, K. Perez, M. Nynka, *et al.*, *Astrophys. J.* **814**, 94 (2015), arXiv:1510.04631 [astro-ph.HE].
- [26] T. Yaqoob, *MNRAS* **423**, 3360 (2012), arXiv:1204.4196 [astro-ph.HE].
- [27] S. Paiano, R. Falomo, A. Treves, and R. Scarpa, *ApJ* **854**, L32 (2018), arXiv:1802.01939 [astro-ph.GA].
- [28] J. M. Dickey and F. J. Lockman, *ARA&A* **28**, 215 (1990).
- [29] P. M. W. Kalberla, W. B. Burton, D. Hartmann, E. M. Arnal, E. Bajaja, R. Morras, and W. G. L. Pöppel, *A&A* **440**, 775 (2005), arXiv:astro-ph/0504140 [astro-ph].
- [30] HI4PI Collaboration, N. Ben Bekhti, L. Flöer, R. Keller, J. Kerp, D. Lenz, B. Winkel, J. Bailin, M. R. Calabretta, *et al.*, *A&A* **594**, A116 (2016), arXiv:1610.06175 [astro-ph.GA].
- [31] F. A. Harrison, W. W. Craig, F. E. Christensen, C. J. Hailey, W. W. Zhang, S. E. Boggs, D. Stern, W. R. Cook, *et al.*, *Astrophys. J.* **770**, 103 (2013), arXiv:1301.7307 [astro-ph.IM].
- [32] F. E. Bauer, P. Arévalo, D. J. Walton, M. J. Koss, S. Puccetti, P. Gandhi, D. Stern, D. M. Alexander, *et al.*, *Astrophys. J.* **812**, 116 (2015), arXiv:1411.0670 [astro-ph.HE].
- [33] S. Marchesi, M. Ajello, L. Marcotulli, A. Comastri, G. Lanzuisi, and C. Vignali, *Astrophys. J.* **854**, 49 (2018), arXiv:1801.03166 [astro-ph.HE].
- [34] I. Georgantopoulos and A. Akylas, *A&A* **621**, A28 (2019), arXiv:1809.03747 [astro-ph.GA].
- [35] A. Pedlar, P. Howley, D. J. Axon, and S. W. Unger, *MNRAS* **259**, 369 (1992).
- [36] A. Zoghbi, J. M. Miller, and E. Cackett, *Astrophys. J.* **884**, 26 (2019), arXiv:1908.09862 [astro-ph.HE].
- [37] V. E. Gianolli, D. E. Kim, S. Bianchi, B. Agís-González, G. Madejski, F. Marin, A. Marinucci, G. Matt, *et al.*, *MNRAS* **523**, 4468 (2023), arXiv:2303.12541 [astro-ph.GA].
- [38] M. J. Koss, B. Trakhtenbrot, C. Ricci, K. Oh, F. E. Bauer, D. Stern, T. Caglar, J. S. den Brok, *et al.*, *ApJS* **261**, 2 (2022), arXiv:2207.12432 [astro-ph.GA].
- [39] K. A. Arnaud, in *Astronomical Data Analysis Software and Systems V*, Astronomical Society of the Pacific Conference Series, Vol. 101, edited by G. H. Jacoby and J. Barnes (1996) p. 17.
- [40] J. Wilms, A. Allen, and R. McCray, *Astrophys. J.* **542**, 914 (2000), arXiv:astro-ph/0008425 [astro-ph].
- [41] V. A. Acciari, T. Aniello, S. Ansoldi, L. A. Antonelli, A. Arbet Engels, M. Artero, K. Asano, D. Baack, *et al.*, *Astrophys. J.* **927**, 197 (2022), arXiv:2202.02600 [astro-ph.HE].
- [42] M. J. M. Marchã and A. Caccianiga, *MNRAS* **430**, 2464 (2013), arXiv:1301.6550 [astro-ph.HE].
- [43] P. A. Evans *et al.*, *A&A* **469**, 379 (2007), arXiv:0704.0128 [astro-ph.HE].
- [44] R. Abbasi, M. Ackermann, J. Adams, J. A. Aguilar, M. Ahlers, M. Ahrens, J. M. Alameddine, C. Alispach, *et al.*, arXiv e-prints, arXiv:2101.09836 (2019), arXiv:2101.09836 [astro-ph.HE].
- [45] S. Ansoldi, L. A. Antonelli, C. Arcaro, D. Baack, A. Babić, B. Banerjee, P. Bangale, U. Barres de Almeida, *et al.*, *ApJ* **863**, L10 (2018), arXiv:1807.04300 [astro-ph.HE].
- [46] K. Murase, *ApJ* **941**, L17 (2022), arXiv:2211.04460 [astro-ph.HE].
- [47] S. Gao, A. Fedynitch, W. Winter, and M. Pohl, *Nature Astronomy* **3**, 88 (2019).
- [48] E. Kun, I. Bartos, J. Becker Tjus, P. L. Biermann, A. Franckowiak, and F. Halzen, *Astrophys. J.* **934**, 180 (2022), arXiv:2203.14780 [astro-ph.HE].
- [49] M. G. Aartsen, M. Ackermann, J. Adams, J. A. Aguilar, M. Ahlers, M. Ahrens, I. A. Samarai, D. Altmann, K. Andeen, T. Anderson, I. Anseau, G. Anton, C. Argüelles, B. Arsoli, J. Auffenberg, *et al.*, *Science* **361**, 147 (2018), arXiv:1807.08794 [astro-ph.HE].
- [50] F. W. Stecker and M. H. Salamon, in *TeV Gamma-ray Astrophysics. Theory and Observations*, edited by H. J. Völk and F. A. Aharonian (1996) pp. 341–355.
- [51] Gopal-Krishna and P. L. Biermann, *MNRAS* **529**, L135 (2024).
- [52] N. S. Kardashev, *Soviet Ast.* **6**, 317 (1962).
- [53] Astropy Collaboration, T. P. Robitaille, E. J. Tollerud, P. Greenfield, M. Droettboom, E. Bray, T. Aldcroft, M. Davis, A. Ginsburg, *et al.*, *A&A* **558**, A33 (2013), arXiv:1307.6212 [astro-ph.IM].
- [54] Astropy Collaboration, A. M. Price-Whelan, P. L. Lim, N. Earl, N. Starkman, L. Bradley, D. L. Shupe, A. A. Patil, L. Corrales, *et al.*, *Astrophys. J.* **935**, 167 (2022), arXiv:2206.14220 [astro-ph.IM].
- [55] F. Halzen, *International Journal of Modern Physics D* **31**, 2230003-8 (2022), arXiv:2110.01687 [astro-ph.HE].
- [56] N. Sahakyan, *Soviet Ast.* **866**, 109 (2018).
- [57] S. Abdollahi, M. Ajello, L. Baldini, J. Ballet, D. Bastieri, J. Becerra Gonzalez, R. Bellazzini, A. Berretta, *et al.*, *ApJS* **265**, 31 (2023).
- [58] R. Svensson, *MNRAS* **227**, 403 (1987).